Icarus 304 (2018) 162–171

Contents lists available at ScienceDirect

Icarus

journal homepage: www.elsevier.com/locate/icarus

Resurfacing asteroids from YORP spin-up and failure

Kevin J. Graves[a,*], David A. Minton[a], Masatoshi Hirabayashi[a], Francesca E. DeMeo[b], Benoit Carry[c]

[a] Purdue University Department of Earth, Atmospheric, & Planetary Sciences, 550 Stadium Mall Drive, West Lafayette, IN 47907, United States
[b] Massachusetts Institute of Technology Department of Earth, Atmospheric & Planetary Sciences 77 Massachusetts Avenue, Cambridge, MA 02139, United States
[c] Laboratoire Lagrange, UNS-CNRS, Observatoire de la Cote d'Azur, Boulevard de l'Observatoire-CS 34229, F-06304 Nice Cedex 4, France

ARTICLE INFO

Article history:
Received 15 February 2017
Revised 12 August 2017
Accepted 21 August 2017
Available online 24 August 2017

Keywords:
Asteroids
Asteroids
Surfaces
Asteroids
Rotation

ABSTRACT

The spectral properties of S and Q-type asteroids can change over time due to interaction with the solar wind and micrometeorite impacts in a process known as 'space weathering.' Space weathering raises the spectral slope and decreases the 1 μm absorption band depth in the spectra of S and Q-type asteroids. Over time, Q-type asteroids, which have very similar spectra to ordinary chondrite meteorites, will change into S-type asteroids. Because there are a significant number of Q-type asteroids, there must be some process which is resurfacing S-type asteroids into Q-types. In this study, we use asteroid data from the Sloan Digital Sky Survey to show a trend between the slope through the g′, r′, and i′ filters, called the gri-slope, and size that holds for all populations of S and Q-type asteroids in the inner solar system, regardless of orbit. We model the evolution of a suite of asteroids in a Monte Carlo YORP rotational evolution and space weathering model. We show that spin-up and failure from YORP is one of the key resurfacing mechanisms that creates the observed weathering trends with size. By varying the non-dimensional YORP coefficient and running time of the present model over the range 475–1425 Myr, we find a range of values for the space weathering timescale, $\tau_{SW} \approx 19$–80 Myr at 2.2 AU. We also estimate the time to weather a newly resurfaced Q-type asteroid into an S-complex asteroid at 1 AU, $\tau_{Q \rightarrow S(1AU)} \approx 2$–7 Myr.

1. Introduction

The most common type of meteorite falls are ordinary chondrites (OCs) (e.g. Chapman, 1996). They have very similar spectral signatures to S-type asteroids, which are the most common type of Near Earth Asteroid (NEA) (Binzel et al., 2004; Carry et al., 2016). Both the asteroids and the meteorites generally have broad 1 and 2 μm absorption bands, as well as a feature at ~1.3 μm, which suggests that they may have similar composition (e.g. Gaffey, 2010). However, their spectra are not a perfect match. S-type asteroid spectra have higher relative reflectance at longer wavelengths through the visible and near infrared, or have higher spectral slopes, compared to Q-type asteroid spectra, and have subdued absorption band depths (DeMeo et al., 2009). Note that S-type asteroids also tend to have lower absolute reflectance compared to Q-types (Binzel et al., 2004). Multiple studies have shown that S-type asteroids are almost certainly the progenitors of many OC meteorites, and the differences in spectral characteristics can be due to a process known as space weathering (Chapman, 2004; Nakamura et al., 2011; Brunetto et al., 2015).

Space weathering is a broad term that is used to describe how ion irradiation from the solar wind and micrometeorite impacts affect the optical properties of material on a surface of an airless body, such as the Moon and asteroids (Brunetto et al., 2015). If a surface starts with an OC composition, space weathering will work to increase the spectral slope and decrease the absorption band depths until its spectrum resembles an S-type asteroid. These changes in spectral parameters have been seen in the grains brought back from asteroid (25143) Itokawa (Noguchi et al., 2011) and in the old vs. freshly exposed regions in the Galileo images of asteroid (243) Ida (Chapman, 1996). The presence of asteroids that are a direct match to some OCs, known as Q-type asteroids, poses an interesting problem. If space weathering alters the surfaces of these asteroids, but there are asteroids present that do not show any sign of space weathering, there must either be a compositional or physical reason keeping certain asteroids from weathering or additional processes that are resurfacing these asteroids.

Hapke (2001) argued for a selective space weathering effect, saying that the solar wind could not weather a surface with an

* Corresponding author.
E-mail address: graves24@purdue.edu (K.J. Graves).

http://dx.doi.org/10.1016/j.icarus.2017.08.025
0019-1035/

OC composition in the absence of fine regolith, potentially giving smaller asteroids, with less fine regolith, a less weathered spectrum. However, observations of S-type asteroid (25143) Itokawa showed highly weathered regions with very little fine regolith (Ishiguro et al., 2007).

Resurfacing processes may be the better solution. These processes could include the catastrophic breakup of an asteroid creating smaller asteroids from its unweathered interior or the removal of a surface layer exposing unweathered underlying material. If resurfacing processes are the primary reason for the existence of Q-type asteroids, the high fraction of small Q-type NEAs (DeMeo et al., 2014) suggests that these processes must, on average, reset a single NEA in a timescale comparable to that of space weathering.

The timescale for space weathering of an asteroid with an OC composition has been estimated from laboratory experiments to take anywhere from 10^3 to 10^8 years. From heavy ion irradiation experiments, Strazzulla et al. (2005) estimated a timescale for the solar wind to raise the spectral slope of an OC to something similar to an S-type asteroid to be $10^4 - 10^6$ years in the NEA region. Loeffler et al. (2009) conducted similar experiments with keV He ions and found a timescale of less than 10^4 years at 1 AU. Sasaki et al. (2001) estimated the timescale for micrometeorite impacts to raise the spectral slope of an asteroid with OC composition to a fully weathered S-type asteroid to be about 10^8 years in the NEA region. Vernazza et al. (2009) matched the ages and spectra of recently created asteroid clusters to the weathering timescales in Strazzulla et al. (2005) to claim that the solar wind is raising the spectral slope of asteroids in the main belt at timescales $\lesssim 10^6$ years, and that micrometeorite impacts continue to slightly increase their spectral slopes through 10^8 years. The rapid weathering timescales of irradiation experiments compared to micrometeorite experiments have led many to believe that the solar wind is the primary space weathering mechanism, especially for relatively unweathered asteroids, such as Q-types. These results may help constrain any mechanism proposed for the resurfacing of asteroids.

Additional constraints on resurfacing mechanisms can be gathered from the distribution of less weathered Q-type asteroids. Q-type asteroids have been primarily found in the NEA region (Binzel et al., 2004, 2010; DeMeo et al., 2014; Carry et al., 2016), but they have also been found in the small members of multiple asteroid families and clusters (Mothé-Diniz and Nesvorný, 2008; Rivkin et al., 2011; Thomas et al., 2011, 2012), and in the members of recently separated asteroid pairs (Polishook et al., 2014a). Marchi et al. (2006a) showed that the spectral slope decreased from a higher average S-type slope to a lower average Q-type slope with decreasing perihelion in the NEA and Mars Crosser (MC) regions. Additionally, Binzel et al. (2004) noted that the average spectral slope of NEAs and MCs decreased with decreasing size, starting at a diameter of ~ 5 km. Carry et al. (2016) and Thomas et al. (2012) found a similar size trend using data from the Sloan Digital Sky Survey (SDSS) in the NEAs and MCs and the Koronis family, respectively. Lin et al. (2015) conducted a multicolor survey and found that the ratio of sub-kilometer Q-type to S-type asteroids in the main belt is < 0.05. However, both Carvano et al. (2010) and DeMeo and Carry (2013) classified the asteroids in the main belt that were observed by the SDSS, and Carvano et al. (2010) found about four times more Q-types than DeMeo and Carry (2013) at sizes $\lesssim 5$ km. Surveys like the SDSS and that of Lin et al. (2015) have only limited spectral resolution, and, more importantly, limited spectral coverage. As many S and Q-type asteroids can be degenerate in the visible wavelengths, observations in both the near infrared and the visible wavelengths are needed to accurately determine the boundary between the taxonomic classes. Due to the limited observations of small main belt asteroids in both the visible and the near infrared, the ratio of Q to S-types in the main belt is not fully understood.

To match the observed trends of unweathered asteroids, resurfacing mechanisms have been proposed. Willman et al. (2008, 2010) and Willman and Jedicke (2011) calculated weathering timescales by assuming that asteroids were resurfaced only after their last catastrophic disruption. Using the ages of asteroid families and the estimated age since last catastrophic disruption (Bottke et al., 2005), they estimated weathering timescales of $10^8 - 10^9$ years. These timescales for the destruction of asteroids into smaller unweathered fragments is 2–5 orders of magnitude longer than the ion irradiation experiments simulating the solar wind. Seismic shaking from smaller, more frequent impacts causing overturn of the surface has been cited as a possible solution to this mismatch in timescales (e.g. Rivkin et al., 2011; Shestopalov et al., 2013).

Studies have used tidal effects from close encounters with the terrestrial planets to explain the high number of Q-type NEAs and the trend of decreasing spectral slope with decreasing perihelion (Nesvorný et al., 2005, 2010; Marchi et al., 2006a; Binzel et al., 2010; DeMeo et al., 2014; Carry et al., 2016). Additionally, thermal cracking of rocks on the surface of asteroids due to diurnal cycling has been recently shown to be a possible mechanism for fresh regolith creation (Delbo et al., 2014; Molaro et al., 2015). Rocks that are broken down could expose unweathered surfaces, and could also potentially explain the trend of decreasing spectral slope with decreasing perihelion.

Finally, the Yarkovsky-O'Keefe-Radzievskii-Paddack (YORP) effect can cause asteroids to accelerate their spin rates until they reach a state of fission or large-scale failure, potentially resurfacing the asteroid (Rubincam, 2000; Vokrouhlický et al., 2015). The YORP effect is the change in rotation rate and obliquity of an asteroid due to thermally induced torques generated from a non-symmetric shape (Rubincam, 2000; Vokrouhlický et al., 2015). The effect of YORP spin-up and failure on the spectra of S and Q-type asteroids has not been studied in detail.

To date, the most successful modeling attempts to explain the presence and distribution of Q-types have been from the close encounter hypothesis. Binzel et al. (2010) and Nesvorný et al. (2010) showed that the orbits of Q-type asteroids could be correlated primarily with encounters from Earth or Venus. Nesvorný et al. (2010) noted that they were only able to match the overall number of Q-type asteroids and not their orbital distribution. They found that they could match the fraction of Q-types with either high (> 1.5 AU) or low ($\lesssim 1$ AU) semi-major axis, but not both. DeMeo et al. (2014) reported further observations and found Q-type asteroids that were in orbits that only crossed the orbit of Mars, and suggested that Mars could also be effective in resurfacing asteroids. However, using observations from the SDSS, Carry et al. (2016) showed that both S-type and Q-type asteroids have similar probabilities of having a close encounter with Mars. Another resurfacing mechanism may be required to explain unweathered asteroids in the MC region. Additionally, the close encounter hypothesis does not require that more Q-type asteroids are found at smaller sizes. An explanation that naturally accounts for the presence of Q-type asteroids in the MC region and at small sizes is desirable.

In this study, we model the effect of YORP spin-up and failure to explain the trend of decreasing spectral slope with decreasing size. The acceleration rate of the spin of an asteroid by the YORP effect is (Scheeres, 2007; Rossi et al., 2009):

$$\dot{\omega} = \frac{3BG_1}{4\pi\rho a^2\sqrt{1-e^2}}\frac{1}{R^2}C_y \tag{1}$$

where $B \approx 2/3$ is the Lambertian scattering coefficient, $G_1 \approx 10^{17}\,\mathrm{kg\,m/s^2}$ is the solar radiation constant, ρ is the

density of the asteroid, C_y is a non-dimensional YORP coefficient, R is the volumetric mean radius of the asteroid, and a and e are its semi-major axis and eccentricity. The C_y parameter describes the effectiveness of YORP on a particular asteroid, and contains information of its shape and moments of inertia. The asteroid's spin rate will accelerate toward a maximum allowed spin rate if $C_y > 0$ and will decelerate toward a zero spin rate if $C_y < 0$. Due to the dependence of the acceleration rate on a and R, we expect YORP to become more important at small sizes close to the sun.

Recently, Golubov and Krugly (2012) studied the effects of the normal and tangential components of the solar radiation pressure on the YORP torque and found that the magnitude of these components are on a similar order. Our model is based on the normal component only.

If space weathering is dominated by the solar wind, the rate of exposure will also increase closer to the sun (Marchi et al., 2006b):

$$\text{exposure rate} \propto \frac{1}{a^2\sqrt{1-e^2}} \tag{2}$$

Increasing the amount of exposure to the solar wind will continue to change the spectral properties of S and Q-type asteroids until they saturate as a fully weathered S-type. If asteroids are resurfaced by YORP and weathered by the solar wind, we expect to find lower spectral slopes and more Q-type asteroids at smaller sizes, regardless of orbital location, addressing shortcomings of the close encounter models.

We organize this paper as follows. In Section 2, we show that the weathering states of S and Q-type asteroids are qualitatively consistent with YORP spin-up and failure. We show that their weathering states have a similar dependence on the size of the asteroid, regardless of its orbital location. In Section 3, we develop a YORP spin-up, resurfacing, and space weathering model and match the slope of the linear regression through the g′, r′, and i′ filters of the SDSS data, called the gri-slope, for a range of asteroid sizes of Flora family asteroids. In Section 4, investigate the effects of assumptions made in the nominal model. We discuss these results in Section 5.

2. Orbitally independent gri-slope vs. size trend

Multiple mechanisms - including YORP spin up and failure and collisions followed by seismic shaking - would cause a size dependence in the weathering state of S and Q-type asteroids. Unweathered asteroids are more common at small sizes in the NEAs, MCs, and in members of particular asteroid families (Binzel et al., 2004; Thomas et al., 2012; Carry et al., 2016). Using data generated from the SDSS, we show that the correlation between low spectral slopes and size is pervasive throughout the inner solar system.

The Sloan Digital Sky Survey is a large photometric and spectroscopic survey that was primarily designed to observe extragalactic objects (York et al., 2000). The SDSS also detects moving objects, such as asteroids in the main belt, NEA and MC regions (Ivezić et al., 2001; Carry et al., 2016). The SDSS takes observations in five photometric bands in the visible wavelengths. These five bands have been used to sort asteroids into broad taxonomic classes (Carvano et al., 2010; DeMeo and Carry, 2013; Carry et al., 2016). In this study, we use the set of SDSS data that was processed and classified by DeMeo and Carry (2013) and Carry et al. (2016).

Classifying asteroids as either Q-types or S-types is difficult without both visible and near-infrared spectral data. Additionally, the majority of Sk and Sq-type asteroids in the main belt are good matches to some OC meteorites (Mothé-Diniz et al., 2010). A resurfaced asteroid with this composition need not be classified as a Q-type. To avoid these difficulties, we only use the gri-slope as a parameter to describe the amount of weathering that has accumulated on the surface (DeMeo and Carry, 2013). The gri-slope is qualitatively the same as the spectral slope. In most cases, a higher gri-slope will correspond to a higher spectral slope and a more weathered surface.

In Fig. 1, we plot the distribution of the gri-slopes of all observed main belt S and Q-type asteroids as a function of their size. We show the linear regression through all asteroids with

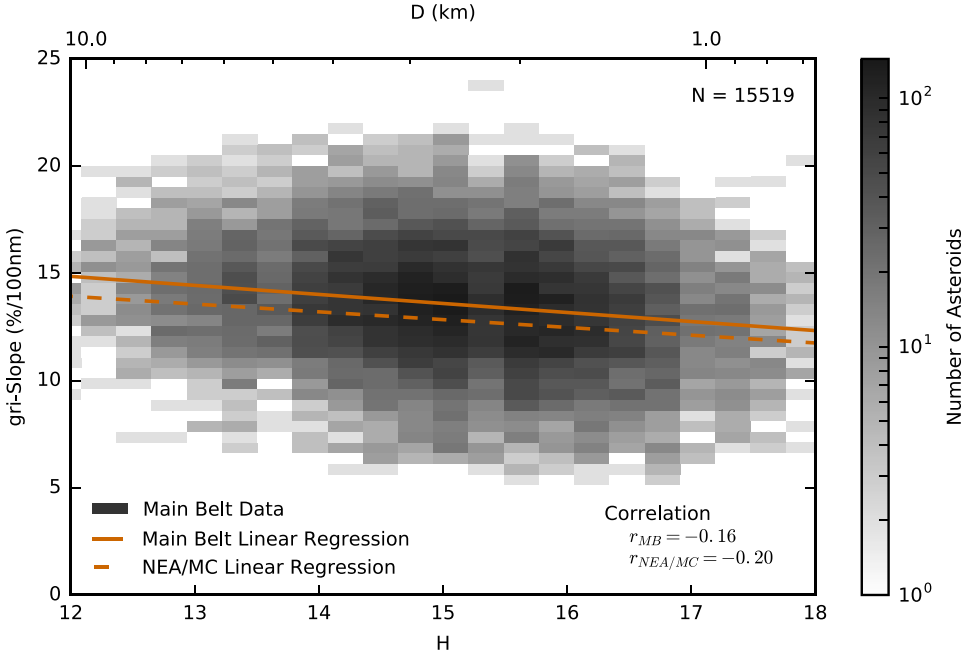

Fig. 1. The distribution of gri-slope vs. absolute magnitude of S and Q-type asteroids in the main belt from the SDSS. The solid line is the linear regression through the main belt asteroids with absolute magnitudes H > 13, and the dashed line is the linear regression through the NEA and MC data from Carry et al. (2016) (data not shown). The slopes of the linear regressions are -0.42 ± 0.04%/100 nm/mag and -0.36 ± 0.17%/100 nm/mag for the main belt asteroids and NEA and MC asteroids, respectively, showing a statistically significant decrease in the average gri-slope of asteroids smaller than H=13 for both populations.

an absolute magnitude H > 13 (approximately diameters D < 5 km). Choosing the cutoff of D < 5 km is consistent with the change in the trend of gri-slopes vs. size seen in the Koronis family (Thomas et al., 2012), as well as the maximum size of detected Q-type asteroids (Binzel et al., 2004). Also, the slope of the linear regression of only the asteroids with a magnitude of $H < 13$ is statistically insignificant. This suggests that a resurfacing mechanism is only present at sizes H $\gtrsim$ 13. We also include the linear regression of the NEA and MC S and Q-type asteroids generated from the data shown in Fig. 7 of Carry et al. (2016).

Both the main belt and the NEA and MC asteroids have nearly the same trend of decreasing average gri-slopes with decreasing size. The slopes of the linear fits are -0.42 ± 0.04%/100 nm/mag and -0.36 ± 0.17%/100 nm/mag for the main belt asteroids and NEA and MC asteroids, respectively. There is a vertical offset between the linear regression of the main belt and NEA and MC data of 0.6 ± 0.3 %/100 nm/mag. At all sizes, NEAs and MCs have, on average, slightly lower gri-slopes than their main belt counterparts, but there is a similar trend in both populations.

Composition can also affect the observed gri-slope of individual asteroids (Sasaki et al., 2002; Marchi et al., 2005). The fraction of olivine to pyroxene can cause different maximum (minimum) gri-slopes for fully weathered (unweathered) objects as well as different weathering rates. By considering the entire main belt, we effectively ignore compositional effects. To remove any effect of composition, we can restrict ourselves to a single asteroid family.

The Flora family is a good test population to investigate the resurfacing of asteroids. It is an old family (Dykhuis et al., 2014), so the weathering states of all family members should not be greatly affected by the initial family-forming collision. Its location in the inner belt allows smaller asteroids to be detected by the SDSS. The composition of the Flora family is expected to be dominated more by olivine than pyroxene, potentially allowing for a greater range in gri-slopes between weathered and unweathered surfaces (Vernazza et al., 2009). Finally, asteroids in the Flora family do not cross the orbits of the terrestrial planets, avoiding any need to disentangle the effects of resurfacing due to planetary encounters.

In Fig. 2, we plot the gri-slope vs. size for the members of the Flora family using the asteroid family catalog of Nesvorný et al. (2015). We again plot the linear regression through all asteroids with a magnitude H > 13. We also include the running mean of the gri-slopes, with a box size of 15 and the uncertainty of the mean values at a 95% confidence level. There is a steeper gri-slope vs. size trend in the Flora family when compared to the entire main belt. The slope of the linear regression of the gri-slopes vs. size for the Flora family is -0.73 ± 0.15%/100 nm/mag. The steeper trend may be due to the large olivine content of the Flora family asteroids (Vernazza et al., 2009). We only use the data from the Flora family to compare to our modeling results later in this paper.

We claim that any results from the restricted analysis of the Flora family are generally applicable to the entire inner solar system due to the similarity of the NEA and MC, and main belt trends shown in Fig. 1. The MCs, which are the majority of asteroids observed in Carry et al. (2016), are sourced from weak resonances all throughout the main belt (Morbidelli and Nesvorný, 1999). Thus, we can expect the MCs to have the same compositional trends as the main belt. We also find qualitatively similar gri-slope vs. size trends if we consider the NEAs or the inner, middle, or outer main belt asteroids alone.

YORP spin-up and failure coupled with space weathering from the solar wind qualitatively fits the data in Figs. 1 and 2. The YORP effect and exposure from the solar wind scale identically with orbit, but only YORP will work increasingly effectively to resurface asteroids at smaller sizes. Additionally, the large sensitivity of the YORP effect from the exact placement of boulders and craters on the surface can cause a large range of possible rotational acceleration rates (Statler, 2009), giving a spread in the timescales needed for an asteroid of a particular size to spin up to the point of failure. A spread in timescales for an asteroid to fail and resurface would also generate a spread in the gri-slopes as seen in Figs. 1 and 2. In the next section we develop a model to test the parameters needed for YORP to create the gri-slope vs. size trend seen in Fig. 2.

3. Nominal YORP spin-up and failure model

To understand the process of resetting a surface from YORP spin-up and failure, we develop a Monte Carlo code to compute the evolution of the spin rate and the weathering rate for a population of asteroids. Our YORP evolution model is similar to published models that reproduced the rotation rate of NEAs and main belt asteroids and the size distribution of main belt asteroids (Rossi et al., 2009; Marzari et al., 2011; Jacobson et al., 2014).

In our model, we simulate 10^4 asteroids for 950 Myr, corresponding to the age of the Flora family (Dykhuis et al., 2014). For each asteroid, we select an absolute magnitude from a uniform distribution of 12 < H < 18. We only consider the trends based on size, so we do not replicate the size frequency distribution of the asteroid population. We select the initial rotation rate from a Maxwellian distribution with $\sigma \approx 2$ rev/day. The spin rates of small asteroids deviate from a Maxwellian distribution for sizes less than $D \approx 5$ km (Polishook and Brosch, 2009); however, due to the strong effect of YORP on the evolution of small asteroids, the initial rotation rate distribution has no effect on the end state in a YORP evolution model (Rossi et al., 2009).

We assume that all asteroids begin with unweathered surfaces. The initial weathering state of their surfaces is also a transient effect that does not affect the end state of these simulations. We assume that the asteroids in our model can be represented by prolate ellipsoids. We draw an aspect ratio b/a of the smaller to largest axis for each asteroid from a Gaussian distribution with a mean of $\mu = 0.6$ and a standard deviation of $\sigma = 0.18$ following Jacobson et al. (2014), which matches the aspect ratio of small, fast-rotating asteroids (Michikami et al., 2010). We calculate the maximum allowed spin rate before failure from a simplified model using the aspect ratio (Pravec and Harris, 2000):

$$\omega_{max} \approx \sqrt{\frac{4\pi \rho G}{3} \frac{b}{a}} \tag{3}$$

where ρ is the density of the asteroid and G is the gravitational constant. We set the density of all asteroids to $\rho = 2500$ kg/m^3.

We do not consider the effect of cohesive forces on asteroid failure in our model. Asteroids larger than approximately 200 m almost never rotate faster than 2.2 h, the critical spin rate for a spherical asteroid held together only by gravity (Pravec and Harris, 2000). Because our model only considers asteroids down to a size of $H = 18$ ($D \approx 700$ m), cohesion should have little effect on the failure rate of these bodies.

At each timestep, every asteroid is spun up by YORP and is weathered by a simplified space weathering model. We evolve the asteroid spin rate by Eq. (1). Following Jacobson et al. (2014), we draw the YORP coefficient C_y from a Gaussian distribution centered at zero with a standard deviation of $\sigma = 0.0125$. The standard deviation is approximated from calculated values of C_y from observed asteroids (Scheeres, 2007).

We do not consider YORP obliquity evolution in our model. The combined obliquity and spin evolution of an asteroid is complex. YORP will cause an asteroid to asymptotically evolve toward a single obliquity value while increasing or decreasing its spin rate (Vokrouhlický and Čapek, 2002; Bottke et al., 2006). Our values of the YORP parameter C_y are derived from observations with a large range of obliquities and are normalized to an obliquity

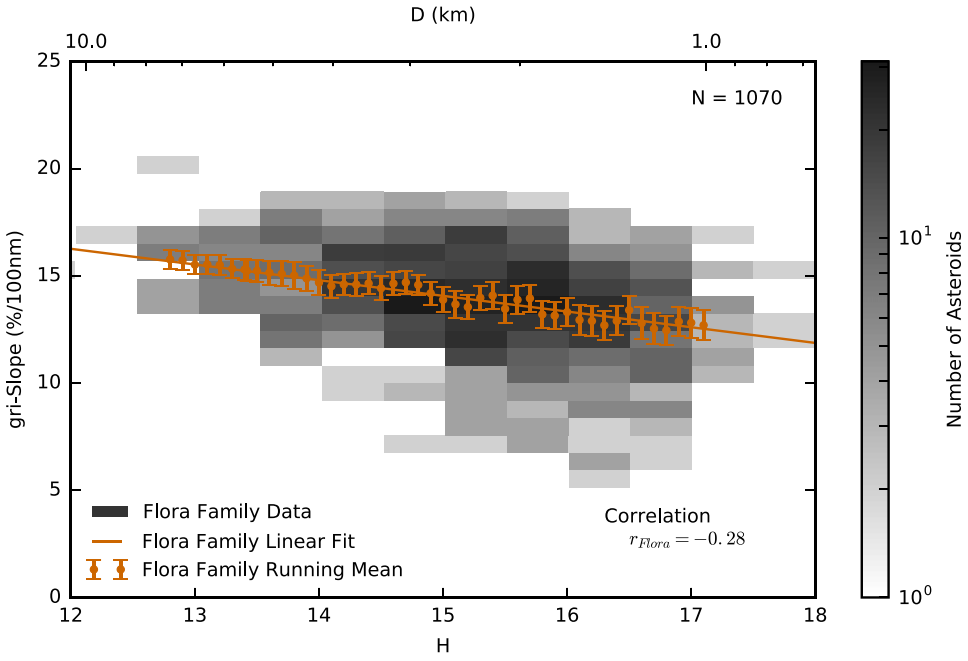

Fig. 2. Same as Fig. 1, except only considering asteroids in the Flora family. The solid line is the linear regression through the Flora family asteroids with absolute magnitudes H > 13. The points and error bars are the running mean of the gri-slope with a box size of 15 and the uncertainty of the mean values at a 95% confidence level. The slope of the linear regression is -0.73 ± 0.15%/100 nm/mag, showing a significant decrease in the average gri-slope of asteroids smaller than H = 13 that is steeper than the trends in Fig. 1.

of 90° (Scheeres, 2007). Since an obliquity of 90° often generates the largest absolute value of rotation rate acceleration (e.g. Bottke et al., 2006), we can expect our range of C_y values for the population will incorporate the appropriate range of possible values. Without obliquity dynamics, the evolution of individual asteroids will not be valid, but we can estimate that, for a population of asteroids, the average timescale between resurfacing events will be accurate.

We incrementally weather the asteroids with a simplified space weathering model. We track the time, t, since the last resurfacing event for each asteroid, and calculate a corresponding gri-slope for the asteroid:

$$S = (S_{max} - S_Q)(1 - \exp(-t/\tau_{SW})) + S_Q \quad (4)$$

where S_{max} is the maximum gri-slope an S-type asteroid attains, S_Q is the gri-slope of a freshly exposed Q-type asteroid, and τ_{SW} is the timescale of the weathering. Eq. (4) is a saturation curve and has been used to fit optical properties of an asteroid's surface from the accumulation of space weathering (Brunetto et al., 2006; Willman et al., 2010).

When the spin rate of an asteroid reaches the maximum spin rate, defined by Eq. (3), the asteroid experiences a resurfacing event. The resurfacing event could be due to fission, or a large scale surface disruption from global landslides. Regardless of the exact process, we consider the asteroid to be resurfaced. We set the time since last resurfacing event $t = 0$, and reselect a new YORP coefficient with the condition that $C_y < 0$. We keep the size and aspect ratio of the asteroid the same. We also make the reasonable assumption that an event that completely resurfaces an asteroid would also change the overall shape of the asteroid, so we also select a new random value of C_y. It is important to note that, depending on how an asteroid's surface fails at high spin rates, it may be possible for the overall shape of the asteroid to change without a total resurfacing event. We discuss the possibility and effects of an incomplete resurfacing event in Section 4.

As an asteroid evolves to a low rotation rate, the asteroid can enter into a tumbling state. The evolution in a tumbling state cannot be represented by our simple model. Following Jacobson et al. (2014), we apply a minimum spin rate of 10^5 hours, at which we reverse the sign of C_y and allow the asteroid's spin rate to accelerate again.

We do not consider collisions in our model. Previous models have used collisions as an additional mechanism to evolve the spin rate of asteroids and have been necessary to describe the rotation rate distribution of the main belt (Marzari et al., 2011). In our model we are primarily concerned with relative timescales of weathering and resurfacing of asteroids. Collisions cause infrequent stochastic evolution in the spin rates of the asteroids, but the spin rates of small asteroids are primarily dominated by YORP (Marzari et al., 2011). The stochastic evolution generated from collisions can cause some interesting second order effects which we will discuss in the next section, but they do not substantially change the results of our modeling.

Using the Flora family SDSS data (Fig. 2), we set the values of some of the parameters in Eqs. 1 and 4. From the location of the Flora family in the inner main belt, we set $a = 2.2$ AU and $e = 0$ in Eq. (1). We also make the assumption that the space weathering timescale, described in Eq. (4), is dominated by the solar wind. The solar wind has an dependence on the orbit shown in Eq. (2), so the timescale of space weathering τ_{SW} is dependent on our choice of a and e. We can use Eq. (2), to scale the space weathering timescale to other values of a and e.

We derive the maximum gri-slope, S_{max}, from a normal distribution based on the distribution of Flora family asteroids with magnitudes of H < 13. For the Flora family members, we find an average value of 15.9%/100 nm and a standard deviation of 1%/100 nm. We selected S_Q from a normal distribution with an average of 6%/100 nm and a deviation of 0.5%/100 nm, which corresponds to the lower end of the range of gri-slopes for Q-types in the DeMeo and Carry (2013) classification scheme.

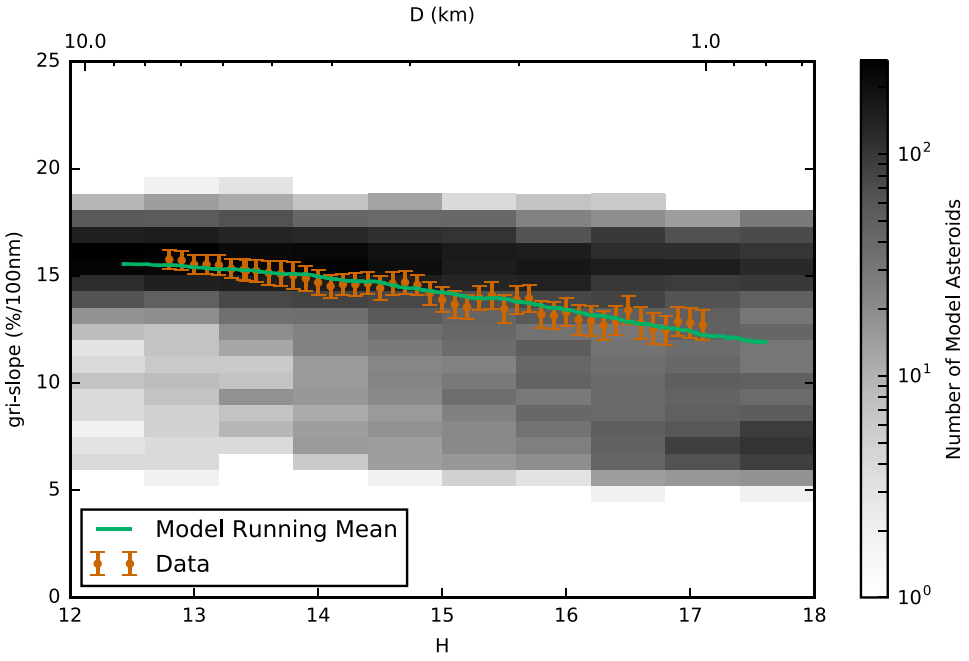

Fig. 3. The modeled asteroids' gri-slope vs. absolute magnitude distribution for the best fit solution with an e-folding space weathering timescale of $\tau_{SW} = 45$ Myr at 2.2 AU. The points and error bars are the running mean of the gri-slope with a box size of 15 and the uncertainty at a 95% confidence level of the Flora family asteroids (from Fig. 2). The solid line is the running mean of the gri-slope of the modeled data with a box size of 330. The uncertainty of the mean for the model data is smaller than the thickness of the line.

With the assumptions made above, the space weathering timescale τ_{SW} is the only free parameter in our model. Due to the form of our space weathering model, space weathering will asymptotically approach S_{max} with an e-folding time τ_{SW}. We vary τ_{SW} in our model to find the best fit. Fig. 3 shows a good fit for $\tau_{SW} = 45$ Myr. We show the gri-slope vs. absolute magnitude distribution of the model results, along with the running mean of both the model results (box size of 330) and the data from the Flora family from Fig. 2.

We also find a range of space weathering timescales that acceptably fit the distribution. In Fig. 4, we show the Root Mean Square Error (RMSE) between the running mean of the observed and modeled asteroids. The box sizes of the running means were chosen to approximately select from the same range of H values, but the RMSEs are insensitive to small variations in the box size. We used the average uncertainty of the mean values of the Flora family asteroids of ±0.58%/100 nm as a cutoff to define the best fit RMSEs. We found a range of space weathering timescales, $\tau_{SW} = 32 - 70$ Myr, where the RMSE $\leq$ 0.58%/100 nm.

To make these results more comparable to previous studies, we can estimate the time it takes for a newly resurfaced Q-type asteroid to weather such that it would become an S-complex asteroid, $\tau_{Q\rightarrow S}$. From DeMeo and Carry (2013), the maximum slope a Q-type asteroid can have is 9.5%/100 nm. We find the average time that it takes to weather an asteroid from a newly resurfaced state, with a gri-slope of $\sim$ 6%/100 nm, to a state where the gri-slope is 9.5%/100 nm. From our range of estimates for the space weathering timescale, we estimate $\tau_{Q\rightarrow S} \approx 14 - 31$ Myr. These timescales should only be taken as an approximate maximum, as S-type asteroids can have gri-slopes as low as 6%/100 nm in the classification of DeMeo and Carry (2013). It is the combination of a low gri-slope and a low z′-i′ color (corresponding to a deep 1 μm absorption band) that defines the unweathered Q-types. Additionally, we can scale these timescales to any orbit using Eq. (2):

$$\tau_{Q\rightarrow S} = \tau_0 \cdot \left(\frac{a}{1\ \text{AU}}\right)^2 \sqrt{\left(1 - e^2\right)} \tag{5}$$

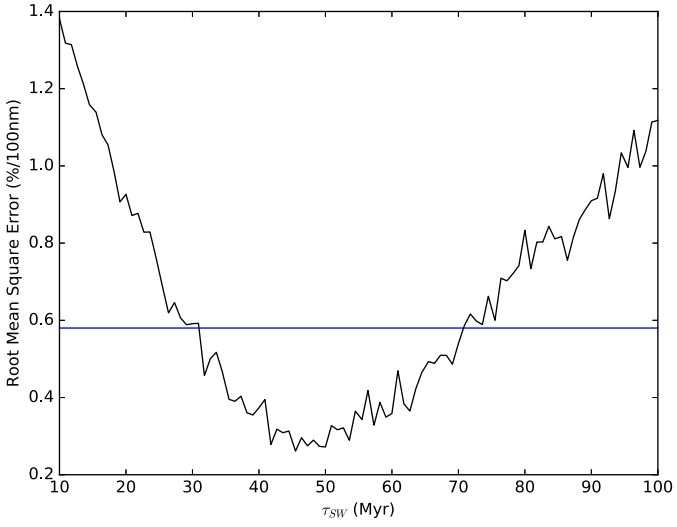

Fig. 4. The Root Mean Square Error (RMSE) of the gri-slope vs. size running mean of the Flora family and the modeled asteroids. The box sizes of the running mean of the observed and modeled asteroids are selected to sample the approximately the same range of absolute magnitudes. We use the average uncertainty of the mean values of the Flora family asteroids of ±0.58%/100 nm as a cutoff to define the best fit RMSEs. The range of acceptable space weathering timescales from the nominal model is $\tau_{SW} = 32 - 70$ Myr, where the RMSE $\leq$ 0.58%/100 nm.

where $\tau_0 \approx 3 - 6$ Myr. In the next section, we address the effects of the assumptions that we use in our nominal YORP spin-up and failure model.

4. Testing assumptions of nominal model

In the construction of our nominal model we made necessary assumptions and selected parameters that have been previously used in the literature. In this section, we discuss and vary the parameters and assumptions made in the nominal model.

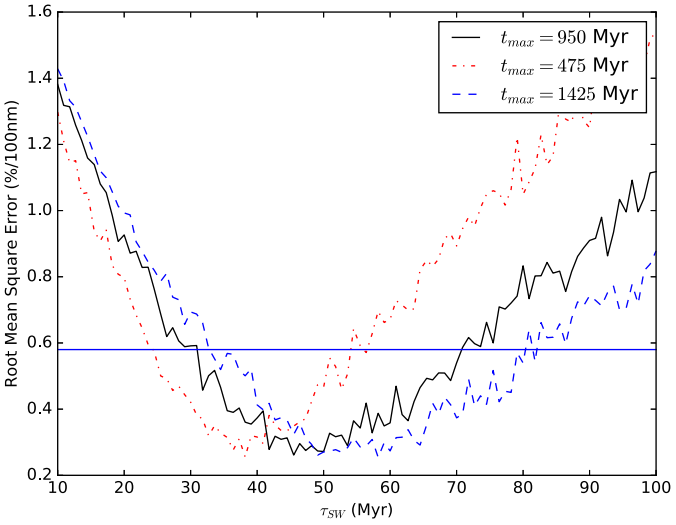

Fig. 5. Similar to Fig. 4, except that we show results from the altering the maximum time, $t_{\max}$, of the model. A larger $t_{\max}$ will allow the population to further evolve toward smaller values of C_y and allow for more rapid YORP evolution, and vice versa for lower values of $t_{\max}$. The change to the τ_{SW} is relatively minor for reasonable values of $t_{\max}$, especially for the minimum bound of τ_{SW}.

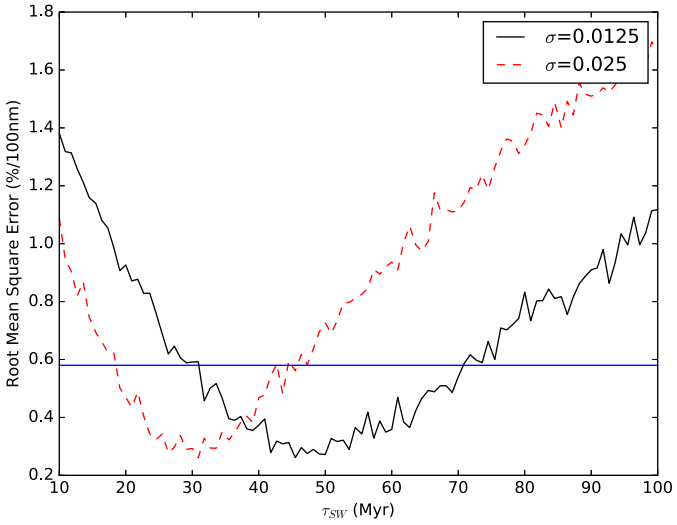

Fig. 6. Similar to Fig. 4, except that we also show results from doubling the standard deviation of the distribution of C_y. A wider distribution of C_y, allows asteroids to evolve more quickly and resurface more often, lowering the acceptable values of τ_{SW}.

An important effect in the model is that the distribution of the YORP coefficients is not in steady state throughout the simulation. As asteroids evolve to the maximum spin rate, and a resurfacing event occurs, their YORP coefficients are randomly redrawn. However, for a given asteroid size, those with a larger absolute C_y values will evolve more quickly and change their C_y values more often. Over time, more asteroids will get "stuck" with low C_y values. Additionally, this trend toward lower values of C_y is more pronounced for smaller asteroids due to their more rapid YORP evolutions. Asteroids that are stuck in these low C_y states will evolve more slowly and lengthen the timescale between resurfacing events, slightly raising the average gri-slopes for smaller asteroids. These low C_y states for small asteroids are important to match the Flora family distribution of gri-slopes at all sizes. Without the slight raising of the average gri-slopes for smaller asteroids, there would be an overabundance of asteroids with very low gri-slopes at small sizes ($H \gtrsim 16$).

The effect of the trend toward lower values of C_y on the derived necessary space weathering timescale is minor. We test the effect of this trend by altering the length of our simulations, $t_{\max}$. In Fig. 5, we show the distribution of the RMSE between the running mean of the model and observations for a range of space weathering timescales and for different values of $t_{\max}$. For lower values of $t_{\max}$, the trend toward lower values of C_y, is muted and restricted to only the smallest asteroids, resulting in shorter resurfacing timescales and requiring a shorter space weathering timescale. By increasing $t_{\max}$, asteroids will have more resurfacing events and causes slightly more asteroids in the simulation to be "stuck" with low C_y values, resulting in longer resurfacing and space weathering timescales. If $t_{\max}$ becomes too small ($\sim$100 Myr), the initial weathering state of the asteroids begins to become important. Varying the nominal value of $t_{\max}$ by $\pm$50% only slightly changes the minimum bound of τ_{SW}. The maximum bound of τ_{SW} does change more significantly. Raising $t_{\max}$ by 50% raises the maximum bound of τ_{SW} to $\approx$80 Myr, and lowering $t_{\max}$ by 50% lowers the maximum bound of τ_{SW} to $\approx$54 Myr.

For asteroids to get stuck with low C_y values, the population must be left undisturbed for a period of time equal to $t_{\max}$. Collisions can create large craters and move boulders on the surface of asteroids, which can cause a significant change in the YORP coefficient (Statler, 2009). This high sensitivity of YORP to the exact shape of the asteroid, called Stochastic YORP (Bottke et al., 2015), could cause small collisions to disturb the asteroids with low values of C_y, thereby increasing C_y, and allowing those asteroids to resurface more often. Marzari et al. (2011) first used collisions alongside YORP evolution. They considered that collisions could effectively induce stochastic evolution by randomly selecting a new C_y after any collision changed the obliquity of the asteroid by >0.2 radians. They found that collisions could trap large ($\approx$5 km) asteroids in a low spin state, which could lengthen the time between resurfacing events. This effect quickly becomes less important at sizes less than 5 km, as YORP begins to more strongly dominate the spin evolution of the asteroid. Since $\approx$5 km is where the trend in decreasing gri-slope with decreasing size begins, we assume that this effect will only cause a minor change in the average gri-slopes of asteroids in our model.

Collisions could potentially decrease the average gri-slope of the smaller asteroids in our model, where the trend toward lower values of C_y is the strongest. Collisions could change C_y often enough to quickly remove any asteroid stuck in a low C_y state, which would keep the time between resurfacing events relatively short. However, the effect of collisions on the evolution of asteroids in our model could be highly dependent on the number of small impactors in the main belt. The exact impactor Size Frequency Distribution (SFD) at sizes $\lesssim$1 km in the main belt is not well understood. Collisional evolution models predict a steep power law slope ($N(>D) \sim D^{-3.5}$) and many small impactors (Dohnanyi, 1969; Bottke et al., 2005). The SDSS and the Sub-Kilometer Asteroid Diameter Survey (SKADS), suggest a shallow power law slope ($N(>D) \sim D^{-2.5}$) continuing down to sizes $D \sim$200 m (Ivezić et al., 2001; Gladman et al., 2009). The rotational disruption model of Jacobson et al. (2014) creates an SFD that also matches well with the shallower power law slope of these observations. A shallower power law could mean less impactors at small sizes, and a slower removal of asteroids stuck with low values of C_y. Regardless of the impact rate, collisions should only affect the resurfacing rate of the smaller ($D \lesssim 2$ km) asteroids. Larger asteroids would still resurface at a similar rate and require a similar space weathering timescale to match observations. The complex interaction between collisions and the resurfacing rate of asteroids from failure at high spin rates are left for a future study.

Table 1
Space weathering timescales for different populations of S and Q-type asteroids. Values are calculated with $\tau_0 \approx 4-17$ Myr for the e-folding timescale (τ_{SW}) and $\tau_0 \approx 2-7$ Myr for the Q-type removal timescale ($\tau_{Q\rightarrow S}$). All timescales are calculated with zero eccentricity.

Location	τ_{SW} (Myr)	$\tau_{Q\rightarrow S}$ (Myr)
NEA Region ($a \approx 1$ AU)	4–17	2–7
Inner Main Belt ($a \approx 2.2$ AU)	19–80	8–35
Middle Main Belt ($a \approx 2.7$ AU)	29–120	12–53
Outer Main Belt ($a \approx 3.1$ AU)	38–159	16–69

The only reasonable change to a parameter that could allow for a shorter space weathering timescale in our model would be increasing the value of C_y. Our nominal distribution of C_y matches well with the measured values of 0.022 and 0.005 for asteroids (1862) Apollo (Kaasalainen et al., 2007) and (54509) YORP (Taylor et al., 2007; Lowry et al., 2007), respectively, under the assumption that these asteroids were affected by YORP. As small asteroids settle into low values of C_y in our model, the standard deviation of C_y decreases to ~ 0.006%/100 nm after 950 Myr, about half of the initial value. Any measurements of C_y of asteroids today could be skewed toward these lower values. To test the effect of changing C_y, we run the model where we select C_y from a Gaussian distribution centered at zero with a standard deviation of $\sigma = 0.025$, twice the nominal value. The RMSE values with the new distribution of C_y for a range of space weathering timescales is shown in Fig. 6. Using these larger values of C_y, we estimate that the needed space weathering timescale can be as short as 19 Myr in the main belt, resulting in space weathering timescales of $\tau = \tau_0 \cdot \left(\frac{a}{1\ \mathrm{AU}}\right)^2 \sqrt{\left(1-e^2\right)}$, where $\tau_0 \approx 4-17$ Myr for the e-folding timescale (τ_{SW}) and $\tau_0 \approx 2-7$ Myr for the Q-type removal timescale ($\tau_{Q\rightarrow S}$). Both of these values of τ_0 are generated from the range of possible solutions discussed in this section. Table 1 provides a list of the approximate e-folding and Q-type removal space weathering timescales for the NEA region, and the inner, middle, and outer main belt.

After reaching the maximum spin rate, an asteroid could experience a number of different effects. Some models have shown that asteroids could fission to form a binary or pair at high spin rates (Walsh and Jacobson, 2015). After a fissioning event, the evolution of a binary asteroid can take different pathways, some of which can slow down the spin rate evolution of the asteroid from YORP (Jacobson and Scheeres, 2011), implying that this mechanism could lengthen the timescale between resurfacing events. We expect binary formation to have a higher order effect on the resurfacing rate of asteroids, and we leave its investigation for a future study. Other modeling efforts such as Hirabayashi (2015), have shown that, depending on the internal structure, spherical asteroids could experience large scale failure at high spin rates, which would not necessarily result in a fission. Any large scale failure could alter the shape of the asteroid and change the sign and magnitude of C_y causing the asteroid to decrease its rotation rate.

Regardless of the outcome of the asteroid's surface at its maximum spin rate, we have considered the asteroid to be fully resurfaced in our model. There is a possibility in both the fissioning and non-fissioning cases that the asteroid would not completely resurface. Movement of a fraction of the surface could change the YORP parameter enough to cause the asteroid's rotation rate to decrease, but it would not completely resurface the asteroid and reset its spectral slope. For instance, repeated landslides and internal deformation, such as those hypothesized to create the equatorial ridge on fast rotating "top-shaped" asteroids, such as (66391) 1999 KW4 and (29075) 1950 DA (Walsh et al., 2008; Hirabayashi and Scheeres, 2015), could refresh the material on only a limited part of the asteroid's surface. Also, Polishook et al. (2014b) suggested that a fission event could be followed by the spreading of dust, which coats the primary and secondary in weathered material and covers any exposed unweathered material.

Unfortunately, there is no clear understanding of the surface evolution of asteroids at high rotation rates. For a partial resurfacing due to landslides or internal deformation, it is unclear what fraction of surface material is displaced when an asteroid reaches its maximum spin rate. Additionally, the probability that an asteroid will experience a certain type of evolution - fission, surface shedding, or large-scale deformation - is unknown. Due to the lack of clear understanding of the surface evolution at high spin rates and to keep unconstrained parameters to a minimum, we only consider the case where an asteroid is fully resurfaced every time it reaches its maximum spin rate.

Previous studies, such as Čapek and Vokrouhlický (2004), Golubov and Krugly (2012), and Bottke et al. (2015), have investigated a bias of YORP torques toward either prograde or retrograde. Unfortunately, these investigations have not converged to a single conclusive answer. We do not account for any YORP directional bias in our model.

5. Discussion

Modeling studies of resurfacing mechanisms are very important because they can allow us to find a range of space weathering timescales at which certain mechanisms are important. By varying parameters in the last section, we find the full range of the space weathering timescale needed for YORP spin-up and failure, $\tau_{SW} \approx 19-80$ Myr. Our estimated Q-type removal timescale, $\tau_{Q\rightarrow S(1AU)} \approx 2-7$ Myr, is shorter than those calculated assuming that disruptive collisions are the primary resurfacing mechanism, but is still longer than laboratory estimates (Willman and Jedicke, 2011; Strazzulla et al., 2005). If the space weathering rate is $\tau_{SW} \sim 1$ Gyr in the main belt as calculated in Willman and Jedicke (2011), from only destructive collisional resurfacing, we would expect YORP spin-up and failure to keep asteroids smaller than a few kilometers uniformly unweathered. This prediction is not consistent with observations, and it suggests that YORP spin-up and failure is a more effective resurfacing mechanism that catastrophic collisions and that the space weathering timescale must be shorter than 1 Gyr.

Laboratory estimates using solar wind as a source find a faster space weathering rate by an order of magnitude or more than what is required for YORP to be the primary resurfacing mechanism for small asteroids. These faster laboratory measurements require one of two things: (1) another mechanism is resurfacing asteroids at a faster rate than YORP spin-up and failure, or (2) the observed space weathering rate is longer than the experimentally derived space weathering rate. A longer observed space weathering rate could be generated from gardening of the surface from small impacts or small landslides as the spin rate and the local slopes on the asteroid change. These local resurfacings would expose unweathered material, giving the asteroid a less weathered overall spectrum, and increasing the time for an asteroid to become saturated (Shestopalov et al., 2013). We also find our estimated space weathering timescale to be comparable ($\sim 2-7$ times longer) than the timescale needed for planetary encounters to create the 20% of Q-types seen in the NEA population from the model of Nesvorný et al. (2010). It is possible that both could be effective resurfacing mechanisms in the NEA region.

There are also other effects apart from YORP spin-up and failure that could cause the spectral slope vs. size trend seen in the data. Collisions and subsequent seismic shaking have been cited as a possible explanation for the similar trend seen in the Koronis Family (Rivkin et al., 2011; Thomas et al., 2011, 2012).

Rivkin et al. (2011) used an order of magnitude argument to suggest that the timescales for collisions and seismic shaking, and space weathering are comparable. It is unclear whether seismic shaking could match the slope and shape of gri-slope vs. size trend or whether that resurfacing rate would be faster or slower than YORP. Its investigation is left for future work.

We discussed in the last section that we do not include binary formation in our model; however, since YORP can create both binary and Q-type asteroids, the number of Q-type vs. S-type binaries can hint at the relative lifetimes of Q-type and binary asteroids. A full statistical analysis is left for future work, but even finding binary Q-type asteroids, such as (1862) Apollo (Pravec and Harris, 2007; DeMeo et al., 2014), suggests that a YORP induced fission (and not a close encounter with Earth or Venus) may have been the last event to resurface that asteroid. This prediction is reasonable because a close encounter with a planet would much more readily disrupt the binary before it would disturb the surface of either member. Walsh and Richardson (2008) showed that close encounters can only be expected to create a small fraction of the binaries in the NEA region, making it unlikely that (1862) Apollo formed by tidal effects. The destruction of binary asteroids is most often due to the Binary YORP effect (Ćuk and Burns, 2005; Jacobson and Scheeres, 2011; Walsh and Jacobson, 2015), which will scale in orbit together with YORP and space weathering. However, we only expect YORP and Binary YORP, and not the space weathering rate to scale with size. A strong prediction of this study is that we should observe more Q-types among small binary asteroids compared to larger binaries.

The spectral slope vs. size trend in this study is not the only trend in spectral slopes that is seen for the S and Q-type asteroids. Marchi et al. (2006a) first noted that there is a spectral slope vs. perihelion trend in the NEAs and MCs. It was these observations that led to further investigations of creating Q-type asteroids from close encounters with the terrestrial planets (e.g. Binzel et al., 2010; Nesvorný et al., 2010; DeMeo et al., 2014; Carry et al., 2016). Boulder breakdown from thermal cycling could also work to resurface asteroids in the NEA region and could naturally create the slope vs. perihelion trend (Delbo et al., 2014; Molaro et al., 2015), although further investigations are necessary. Our study has not considered the perihelion trend, and YORP coupled with space weathering originating from the solar wind will not reproduce it. It seems that there must be at least two primary mechanisms resurfacing asteroids: one effect (such as YORP spin-up and failure) creating the spectral slope vs. size trend and another effect creating the slope vs. perihelion trend. Additionally, if the mechanism creating the perihelion trend is independent of size, which would be reasonable for resurfacing from close encounters with the terrestrial planets or from thermal cycling, it could also explain the size-independent lower gri-slopes in the NEAs and MCs compared to the main belt that is seen in Fig. 1.

6. Conclusion

From gri-slopes of main belt asteroids, MCs, and NEAs gathered from the Sloan Digital Sky Survey, we showed that S-type and Q-type asteroids are, on average, less weathered at smaller sizes, regardless of orbital location. We found the slope of the linear trends of the gri-slope vs. absolute magnitude distributions to be -0.42 ± 0.04%/100 nm/mag and -0.36 ± 0.17%/100 nm/mag for the main belt asteroids, and the NEAs and MCs, respectively. The similarity between the trends suggested a common resurfacing mechanism that preferentially reduces the average gri-slopes of S and Q-type asteroids at smaller sizes. Additionally, we presented the gri-slope vs. size distribution of the Flora family asteroids to remove any compositional trends in gri-slope and any observational biases. We found a steeper slope of the linear trend through the Flora family asteroids of -0.73 ± 0.15%/100 nm/mag.

We presented the first resurfacing model from YORP spin-up and failure to explain the weathering trends with size. With a simple YORP evolution and space weathering model, we can fit the observed gri-slope vs. size trend in the Flora family asteroids. By varying the non-dimensional YORP coefficient distribution and the run time of the model, we find a range of values for the space weathering timescale $\tau = \tau_0 \cdot \left(\frac{a}{1\ \mathrm{AU}}\right)^2 \sqrt{\left(1-e^2\right)}$, where $\tau_0 \approx 4-17$ Myr for the e-folding timescale and $\tau_0 \approx 2-7$ Myr for the Q-type removal timescale.

Given the assumptions in our model, we conclude that YORP spin-up and failure is an effective mechanism for resurfacing small asteroids. The relative effectiveness between YORP and other resurfacing mechanisms affecting only small asteroids, such as impacts and subsequent seismic shaking, is left for future work.

Acknowledgements

K. Graves thanks the NASA Earth and Space Science Fellowship (grant number 15-PLANET15F-0121 and 16-PLANET16R-0036) for funding. We thank Seth Jacobson for a valuable discussion. We also thank two anonymous referees for their helpful comments.

References

Binzel, R.P., Morbidelli, A., Merouane, S., DeMeo, F.E., Birlan, M., Vernazza, P., Thomas, C.a., Rivkin, A.S., Bus, S.J., Tokunaga, A.T., 2010. Earth encounters as the origin of fresh surfaces on near-Earth asteroids. Nature 463 (7279), 331–334.
Binzel, R.P., Rivkin, A.S., Stuart, J.S., Harris, A.W., Bus, S.J., Burbine, T.H., 2004. Observed spectral properties of near-Earth objects: results for population distribution, source regions, and space weathering processes. Icarus 170 (2), 259–294.
Bottke, W.F., Durda, D.D., Nesvorný, D., Jedicke, R., Morbidelli, A., Vokrouhlický, D., Levison, H., 2005. The fossilized size distribution of the main asteroid belt. Icarus 175 (1), 111–140.
Bottke, W.F., Vokrouhlický, D., Rubincam, D.P., Nesvorný, D., 2006. The Yarkovsky and YORP effects: implications for asteroid dynamics. Annu. Rev. Earth Planet. Sci. 34 (1), 157–191.
Bottke, W.F., Vokrouhlický, D., Walsh, K.J., Delbo, M., Michel, P., Lauretta, D.S., Campins, H., Connolly, H.C., Scheeres, D.J., Chelsey, S.R., 2015. In search of the source of asteroid (101955) Bennu: applications of the stochastic YORP model. Icarus 247, 191–217.
Brunetto, R., Loeffler, M.J., Nesvorný, D., Sasaki, S., Strazzulla, G., 2015. Asteroid surface alteration by space weathering processes. Asteroids IV 597–616.
Brunetto, R., Romano, F., Blanco, A., Fonti, S., Martino, M., Orofino, V., Verrienti, C., 2006. Space weathering of silicates simulated by nanosecond pulse UV excimer laser. Icarus 180 (2), 546–554.
Čapek, D., Vokrouhlický, D., 2004. The YORP effect with finite thermal conductivity. Icarus 172 (2), 526–536.
Carry, B., Solano, E., Eggl, S., DeMeo, F., 2016. Spectral properties of near-Earth and Mars-crossing asteroids using Sloan photometry. Icarus 268, 340–354.
Carvano, J.M., Hasselmann, P.H., Lazzaro, D., Mothé-Diniz, T., 2010. SDSS-based taxonomic classification and orbital distribution of main belt asteroids. Astron. Astrophys. 510, A43.
Chapman, C.R., 2004. Space weathering of asteroid surfaces. Annu. Rev. Earth Planet. Sci. 32 (1), 539–567.
Chapman, R., 1996. S-type asteroids, ordinary chondrites, and space weathering: the evidence from Galileo's fly-bys of Gaspra and Ida. Meteorit. Planet. Sci. 31, 699–725.
Ćuk, M., Burns, J.A., 2005. Effects of thermal radiation on the dynamics of binary NEAs. Icarus 176, 418–431.
DeMeo, F.E., Carry, B., 2013. The taxonomic distribution of asteroids from multi-filter all-sky photometric surveys. Icarus 226 (1), 723–741.
DeMeo, F.E., Binzel, R.P., Lockhart, M., 2014. Mars encounters cause fresh surfaces on some near-Earth asteroids. Icarus 227, 112–122.
DeMeo, F.E., Binzel, R.P., Slivan, S.M., Bus, S.J., 2009. An extension of the Bus asteroid taxonomy into the near-infrared. Icarus 202 (1), 160–180.
Delbo, M., Libourel, G., Wilkerson, J., Murdoch, N., Michel, P., Ramesh, K.T., Ganino, C., Verati, C., Marchi, S., 2014. Thermal fatigue as the origin of regolith on small asteroids. Nature 508 (7495), 233–236.
Dohnanyi, J.S., 1969. Collisional model of asteroids and their debris. J. Geophys. Res. 74, 2531–2554.
Dykhuis, M.J., Molnar, L., Van Kooten, S.J., Greenberg, R., 2014. Defining the Flora family: orbital properties, reflectance properties and age. Icarus 243, 111–128.
Gaffey, M.J., 2010. Space weathering and the interpretation of asteroid reflectance spectra. Icarus 209 (2), 564–574.

Gladman, B.J., Davis, D.R., Neese, C., Jedicke, R., Williams, G., Kavelaars, J.J., Petit, J.-M., Scholl, H., Holman, M., Warrington, B., Esquerdo, G., Tricarico, P., 2009. On the asteroid belt's orbital and size distribution. Icarus 202, 104–118.
Golubov, O., Krugly, Y.N., 2012. Tangential component of the YORP effect. Astrophys. J. 752 (1), L11.
Hapke, B., 2001. Space weathering from Mercury to the asteroid belt. J. Geophys. Res 106 (E5), 10039.
Hirabayashi, M., 2015. Failure modes and conditions of a cohesive, spherical body due to YORP spin-up. Mon. Not. R. Astron. Soc. 454 (2), 2249–2257.
Hirabayashi, M., Scheeres, D. J., 2015. Stress and failure analysis of rapidly rotating asteroid (29075) 1950 DA. Astrophys. J. Lett. 798, L8.
Ishiguro, M., Hiroi, T., Tholen, D.J., Sasaki, S., Ueda, Y., Nimura, T., Abe, M., Clark, B.E., Yamamoto, A., Yoshida, F., Nakamura, R., Hirata, N., Miyamoto, H., Yokota, Y., Hashimoto, T., Kubota, T., Nakamura, A.M., Gaskell, R.W., Saito, J., 2007. Global mapping of the degree of space weathering on asteroid 25143 Itokawa by Hayabusa/AMICA observations. Meteorit. Planet. Sci. 42 (10), 1791–1800.
Ivezić, Ž., Tabachnik, S., Rafikov, R., Lupton, R.H., Quinn, T., Hammergren, M., Eyer, L., Chu, J., Armstrong, J.C., Fan, X., Finlator, K., Geballe, T.R., Gunn, J.E., Hennessy, G.S., Knapp, G.R., Leggett, S.K., Munn, J.A., Pier, J.R., Rockosi, C.M., Schneider, D.P., Strauss, M.A., Yanny, B., Brinkmann, J., Csabai, I., Hindsley, R.B., Kent, S., Lamb, D.Q., Margon, B., McKay, T.A., Smith, J.A., Waddell, P., York, D.G., 2001. Solar System objects observed in the Sloan Digital Sky Survey commissioning data. Astron. J. 122 (5), 2749–2784.
Jacobson, S.A., Marzari, F., Rossi, A., Scheeres, D.J., Davis, D.R., 2014. Effect of rotational disruption on the size-frequency distribution of the main belt asteroid population. Mon. Not. R. Astron. Soc. 439 (1), L95–L99.
Jacobson, S.a., Scheeres, D.J., 2011. Dynamics of rotationally fissioned asteroids: source of observed small asteroid systems. Icarus 214 (1), 161–178.
Kaasalainen, M., Ďurech, J., Warner, B.D., Krugly, Y.N., Gaftonyuk, N.M., 2007. Acceleration of the rotation of asteroid 1862 Apollo by radiation torques. Nature 446 (7134), 420–422.
Lin, H., Yoshida, F., Chen, Y., Ip, W., Chang, C., 2015. A search for subkilometer-sized ordinary chondrite like asteroids in the main-belt. Icarus 254, 202–212.
Loeffler, M.J., Dukes, C.A., Baragiola, R.A., 2009. Irradiation of olivine by 4 kev He + : simulation of space weathering by the solar wind. J. Geophys. Res. 114 (E3), E03003.
Lowry, S.C., Fitzsimmons, A., Pravec, P., Vokrouhlický, D., Boehnhardt, H., Taylor, P.A., Margot, J.-L., Galád, A., Irwin, M., Irwin, J., Kusnirák, P., 2007. Direct detection of the asteroidal YORP effect. Science 316 (5822).
Marchi, S., Brunetto, R., Magrin, S., Lazzarin, M., Gandolfi, D., 2005. Space weathering of near-Earth and main belt silicate-rich asteroids: observations and ion irradiation experiments. Astron. Astrophys. 443 (3), 769–775.
Marchi, S., Magrin, S., Nesvorny, D., Paolicchi, P., Lazzarin, M., 2006a. A spectral slope versus perihelion distance correlation for planet-crossing asteroids. Mon. Not. R. Astron. Soc. 368 (1), L39–L42.
Marchi, S., Paolicchi, P., Lazzarin, M., Magrin, S., 2006b. A general spectral slope-exposure relation for S-type main belt and near-Earth asteroids. Astron. J. 131 (2), 1138–1141.
Marzari, F., Rossi, A., Scheeres, D., 2011. Combined effect of YORP and collisions on the rotation rate of small main belt asteroids. Icarus 214 (2), 622–631.
Michikami, T., Nakamura, A.M., Hirata, N., 2010. The shape distribution of boulders on asteroid 25143 Itokawa: comparison with fragments from impact experiments. Icarus 207, 277–284.
Molaro, J.L., Byrne, S., Langer, S.A., 2015. Grain-scale thermoelastic stresses and spatiotemporal temperature gradients on airless bodies, implications for rock breakdown. J. Geophys. Res. E 120 (2), 255–277.
Morbidelli, A., Nesvorný, D., 1999. Numerous weak resonances drive asteroids toward terrestrial planets orbits. Icarus 308, 295–308.
Mothé-Diniz, T., Jasmin, F.L., Carvano, J.M., Lazzaro, D., Nesvorný, D., Ramirez, a.C., 2010. Re-assessing the ordinary chondrites paradox. Astron. Astrophys. 514, A86.
Mothé-Diniz, T., Nesvorný, D., 2008. Visible spectroscopy of extremely young asteroid families. Astron. Astrophys. 486 (2), L9–L12.
Nakamura, T., Noguchi, T., Tanaka, M., Zolensky, M.E., Kimura, M., Tsuchiyama, A., Nakato, A., Ogami, T., Ishida, H., Uesugi, M., Yada, T., Shirai, K., Fujimura, A., Okazaki, R., Sandford, S.A., Ishibashi, Y., Abe, M., Okada, T., Ueno, M., Mukai, T., Yoshikawa, M., Kawaguchi, J., 2011. Itokawa dust particles: a direct link between S-type asteroids and ordinary chondrites. Science 333, 1113.
Nesvorný, D., Bottke, W.F., Vokrouhlický, D., Chapman, C.R., Rafkin, S., 2010. Do planetary encounters reset surfaces of near Earth asteroids? Icarus 209 (2), 510–519.
Nesvorný, D., Brož, M., Carruba, V., 2015. Identification and dynamical properties of asteroid families. Asteroids IV 297–321.
Nesvorný, D., Jedicke, R., Whiteley, R.J., Ivezić, Ž., 2005. Evidence for asteroid space weathering from the Sloan Digital Sky Survey. Icarus 173 (1), 132–152.
Noguchi, T., Nakamura, T., Kimura, M., Zolensky, M.E., Tanaka, M., Hashimoto, T., Konno, M., Nakato, A., Ogami, T., Fujimura, A., Abe, M., Yada, T., Mukai, T., Ueno, M., Okada, T., Shirai, K., Ishibashi, Y., Okazaki, R., 2011. Incipient space weathering observed on the surface of Itokawa dust particles. Science (New York, N.Y.) 333 (6046), 1121–1125.
Polishook, D., Brosch, N., 2009. Photometry and spin rate distribution of small-sized main belt asteroids. Icarus 199, 319–332.
Polishook, D., Moskovitz, N., Binzel, R.P., DeMeo, F.E., Vokrouhlický, D., Žižka, J., Oszkiewicz, D., 2014. Observations of "fresh" and weathered surfaces on asteroid pairs and their implications on the rotational-fission mechanism. Icarus 233, 9–26.
Polishook, D., Moskovitz, N., DeMeo, F.E., Binzel, R.P., 2014. Rotationally resolved spectroscopy of asteroid pairs: no spectral variation suggests fission is followed by settling of dust. Icarus 243, 222–235.
Pravec, P., Harris, A., 2000. Fast and slow rotation of asteroids. Icarus 148 (1), 12–20.
Pravec, P., Harris, A., 2007. Binary asteroid population. Icarus 190 (1), 250–259.
Rivkin, A.S., Thomas, C.A., Trilling, D.E., Enga, M.T., Grier, J.A., 2011. Ordinary chondrite-like colors in small Koronis family members. Icarus 211 (2), 1294–1297.
Rossi, A., Marzari, F., Scheeres, D.J., 2009. Computing the effects of YORP on the spin rate distribution of the NEO population. Icarus 202 (1), 95–103.
Rubincam, D.P., 2000. Radiative spin-up and spin-down of small asteroids. Icarus 148 (1), 2–11.
Sasaki, S., Hiroi, T., Nakamura, K., Hamabe, Y., Kurahashi, E., Yamada, M., 2002. Simulation of space weathering by nanosecond pulse laser heating: dependence on mineral composition, weathering trend of asteroids and discovery of nanophase iron particles. Adv. Space Res. 29 (5), 7–3.
Sasaki, S., Nakamura, K., Hamabe, Y., Kurahashi, E., Hiroi, T., 2001. Production of iron nanoparticles by laser irradiation in a simulation of lunar-like space weathering. Nature 410 (6828), 555–557.
Scheeres, D., 2007. The dynamical evolution of uniformly rotating asteroids subject to YORP. Icarus 188 (2), 430–450.
Shestopalov, D., Golubeva, L., Cloutis, E., 2013. Optical maturation of asteroid surfaces. Icarus 225 (1), 781–793.
Statler, T.S., 2009. Extreme sensitivity of the YORP effect to small-scale topography. Icarus 202 (2), 502–513.
Strazzulla, G., Dotto, E., Binzel, R., Brunetto, R., Barucci, M., Blanco, A., Orofino, V., 2005. Spectral alteration of the meteorite Epinal (H5) induced by heavy ion irradiation: a simulation of space weathering effects on near-Earth asteroids. Icarus 174 (1), 31–35.
Taylor, P.A., Margot, J.-L., Vokrouhlicky, D., Scheeres, D.J., Pravec, P., Lowry, S.C., Fitzsimmons, A., Nolan, M.C., Ostro, S.J., Benner, L.A.M., Giorgini, J.D., Magri, C., 2007. Spin rate of asteroid (54509) 2000 PH5 increasing due to the YORP effect. Science 316 (5822), 274–277.
Thomas, C.A., Rivkin, A.S., Trilling, D.E., Grier, J.A., 2011. Space weathering of small Koronis family members. Icarus 212 (1), 158–166.
Thomas, C.A., Trilling, D.E., Rivkin, A.S., 2012. Space weathering of small Koronis family asteroids in the SDSS moving object catalog. Icarus 219 (1), 505–507.
Vernazza, P., Binzel, R.P., Rossi, A., Fulchignoni, M., Birlan, M., 2009. Solar wind as the origin of rapid reddening of asteroid surfaces. Nature 458 (7241), 993–995.
Vokrouhlický, D., Bottke, W.F., Chesley, S.R., Scheeres, D.J., Statler, T.S., 2015. The Yarkovsky and YORP effects. Asteroids IV.
Vokrouhlický, D., Čapek, D., 2002. YORP-induced long-term evolution of the spin state of small asteroids and meteoroids: Rubincam's approximation. Icarus 159, 449–467.
Walsh, K.J., Jacobson, S.A., 2015. Formation and evolution of binary asteroids. Asteroids IV 375–393.
Walsh, K.J., Richardson, D.C., 2008. A steady-state model of NEA binaries formed by tidal disruption of gravitational aggregates. Icarus 193 (2), 553–566.
Walsh, K.J., Richardson, D.C., Michel, P., 2008. Rotational breakup as the origin of small binary asteroids. Nature 454 (7201), 188–191.
Willman, M., Jedicke, R., 2011. Asteroid age distributions determined by space weathering and collisional evolution models. Icarus 211 (1), 504–510.
Willman, M., Jedicke, R., Moskovitz, N., Nesvorný, D., Vokrouhlický, D., Mothé-Diniz, T., 2010. Using the youngest asteroid clusters to constrain the space weathering and gardening rate on S-complex asteroids. Icarus 208 (2), 758–772.
Willman, M., Jedicke, R., Nesvorný, D., Moskovitz, N., Ivezić, Ž., Fevig, R., 2008. Redetermination of the space weathering rate using spectra of Iannini asteroid family members. Icarus 195 (2), 663–673.
York, D.G., Adelman, J., Anderson, J.J.E., Anderson, S.F., Annis, J., Bahcall, N.A., Bakken, J.A., Barkhouser, R., Bastian, S., Berman, E., Boroski, W.N., Bracker, S., Briegel, C., Briggs, J.W., Brinkmann, J., Brunner, R., Burles, S., Carey, L., Carr, M.A., Castander, F.J., Chen, B., Colestock, P.L., Connolly, A.J., Crocker, J.H., Csabai, I., Czarapata, P.C., Davis, J.E., Doi, M., Dombeck, T., Eisenstein, D., Ellman, N., Elms, B.R., Evans, M.L., Fan, X., Federwitz, G.R., Fiscelli, L., Friedman, S., Frieman, J.A., Fukugita, M., Gillespie, B., Gunn, J.E., Gurbani, V.K., de Haas, E., Haldeman, M., Harris, F.H., Hayes, J., Heckman, T.M., Hennessy, G.S., Hindsley, R.B., Holm, S., Holmgren, D.J., Huang, C.-h., Hull, C., Husby, D., Ichikawa, S.-I., Ichikawa, T., Ivezić, Ž., Kent, S., Kim, R.S.J., Kinney, E., Klaene, M., Kleinman, A.N., Kleinman, S., Knapp, G.R., Korienek, J., Kron, R.G., Kunszt, P.Z., Lamb, D.Q., Lee, B., Leger, R.F., Limmongkol, S., Lindenmeyer, C., Long, D.C., Loomis, C., Loveday, J., Lucinio, R., Lupton, R.H., MacKinnon, B., Mannery, E.J., Mantsch, P.M., Margon, B., McGehee, P., McKay, T.A., Meiksin, A., Merelli, A., Monet, D.G., Munn, J.A., Narayanan, V.K., Nash, T., Neilsen, E., Neswold, R., Newberg, H.J., Nichol, R.C., Nicinski, T., Nonino, M., Okada, N., Okamura, S., Ostriker, J.P., Owen, R., Pauls, A.G., Peoples, J., Peterson, R.L., Petravick, D., Pier, J.R., Pope, A., Pordes, R., Prosapio, A., Rechenmacher, R., Quinn, T.R., Richards, G.T., Richmond, M.W., Rivetta, C.H., Rockosi, C.M., Ruthmansdorfer, K., Sandford, D., Schlegel, D.J., Schneider, D.P., Sekiguchi, M., Sergey, G., Shimasaku, K., Siegmund, W.A., Smee, S., Smith, J.A., Snedden, S., Stone, R., Stoughton, C., Strauss, M.A., Stubbs, C., SubbaRao, M., Szalay, A.S., Szapudi, I., Szokoly, G.P., Thakar, A.R., Tremonti, C., Tucker, D.L., Uomoto, A., Vanden Berk, D., Vogeley, M.S., Waddell, P., Wang, S.-i., Watanabe, M., Weinberg, D.H., Yanny, B., Yasuda, N., 2000. The Sloan Digital Sky Survey: technical summary. Astron. J. 120 (3), 1579–1587.